Eur J Nucl Med Mol Imaging (2014) 41:867–877
DOI 10.1007/s00259-013-2658-6

ORIGINAL ARTICLE

Radioimmunotherapy with Tenarad, a ^{131}I-labelled antibody fragment targeting the extra-domain A1 of tenascin-C, in patients with refractory Hodgkin's lymphoma

Luigi Aloj · Laura D'Ambrosio · Michela Aurilio · Anna Morisco · Ferdinando Frigeri · Corradina Caraco' · Francesca Di Gennaro · Gaetana Capobianco · Leonardo Giovannoni · Hans D. Menssen · Dario Neri · Antonio Pinto · Secondo Lastoria

Received: 6 September 2013 / Accepted: 28 November 2013 / Published online: 17 January 2014

Abstract
Purpose The extra-domain A1 of tenascin-C (TC-A1) is highly expressed in the extracellular matrix of tumours and on newly formed blood vessels and is thus a valuable target for radionuclide therapy. Tenarad is a fully human miniantibody or small immunoprotein (SIP, molecular weight 80 kDa) labelled with ^{131}I that is derived from a TC-A1-binding antibody. Previous phase I/II studies with a similar compound (^{131}I-L19SIP) used for radioimmunotherapy (RIT) have shown preliminary efficacy in a variety of cancer types. In this ongoing phase I/II trial, Tenarad was administered to patients with recurrent Hodgkin's lymphoma (HL) refractory to conventional treatments.
Methods Eight patients (four men, four women; age range 19 – 41) were enrolled between April 2010 and March 2011. All patients had received a median of three previous lines of chemotherapy (range three to six) and seven had also undergone autologous stem cell transplantation (ASCT) or bone marrow transplantation. In addition, seven patients received external beam radiation. All patients had nodal disease, constitutional B symptoms and some showed extranodal disease in skeletal bone (four patients), lung (three), liver (two) and spleen (one). Baseline assessments included whole-body FDG PET with contrast-enhanced CT and diagnostic Tenarad planar and SPECT studies. Patients were considered eligible to receive a therapeutic dose of Tenarad (2.05 GBq/m^2) if tumour uptake was more than four times higher than that of muscle.
Results All patients were eligible and received the therapeutic dose of Tenarad. Only one patient developed grade 4 thrombocytopenia and leucocytopenia, requiring hospitalization and therapeutic intervention. All other patients had haematological toxicity of grade 3 or lower, which resolved spontaneously. At the first response assessment (4 – 6 weeks after therapy), one patient showed a complete response, one showed a partial response (PR) and five had disease stabilization (SD). Five patients were given up to three repeated Tenarad treatments. One patient showed SD which then improved to a PR, three showed clinical benefit while maintaining SD and one patient showed disease progression.
Conclusion Tenarad RIT is effective in chemorefractory HL and resulted in objective responses or clinical benefit in the majority of patients. Toxicity was acceptable despite the high load of prior treatments, previous ASCT and multiple Tenarad administrations. Further studies are planned to define the most effective schedule for this type of RIT in HL patients.

Keywords Hodgkin's lymphoma · Radioimmunotherapy · Dosimetry · ^{131}I · Tenascin-C

L. D'Ambrosio · M. Aurilio · A. Morisco · C. Caraco' · F. Di Gennaro · S. Lastoria
Struttura Complessa Medicina Nucleare, Istituto Nazionale Tumori "Fondazione G. Pascale" - IRCCS, Napoli, Italy

F. Frigeri · G. Capobianco · A. Pinto
Struttura Complessa di Ematologia Oncologica, Istituto Nazionale Tumori "Fondazione G. Pascale" - IRCCS, Napoli, Italy

L. Giovannoni · H. D. Menssen
Philogen, SpA, Siena, Italy

D. Neri
Institute of Pharmaceutical Sciences, ETH, Zurich, Switzerland

L. Aloj (✉)
Struttura Complessa di Medicina Nucleare, Istituto Nazionale Tumori "Fondazione G. Pascale" - IRCCS, Via M. Semmola, 80131 Napoli, Italy
e-mail: l.aloj@istitutotumori.na.it

Introduction

Although classic Hodgkin's lymphoma (HL) is a typical example of a curable human cancer, about 20 % of all patients still experience treatment failure and succumb to recurring disease [1, 2]. Overall treatment failures may occur in up to 30 – 35 % of patients with advanced disease and unfavourable prognostic features at presentation [1, 3]. High-dose chemotherapy with autologous stem cell transplant (ASCT) only cures about 50 % of these patients and allogeneic transplantation usually achieves long-term disease-free survival in a low proportion of patients due to the significant toxicity of the procedure [2, 4]. Therefore, treatment of refractory/relapsed HL remains a clinical challenge and appropriate rescue strategies for this patient population, mostly consisting of young adults, have not been developed and remain a largely unmet medical need [5, 6].

The clinical application of radioimmunotherapy (RIT) has greatly expanded in recent years, primarily due to the proven efficacy of two clinically approved anti-CD20 agents, ^{90}Y-ibritumomab tiuxetan (Zevalin) and ^{131}I-tositumomab (Bexxar) for the treatment of indolent B-cell non-Hodgkin's Lymphoma (NHL) [7]. These developments indicated that monoclonal antibodies (MoAbs) could effectively deliver therapeutic doses of radionuclides to specific cancer sites and induce durable clinical responses as single agents [8, 9]. The RIT approach, however, suffers from some limitations. First, there are no fully human or humanized MoAbs currently approved for RIT and the high immunogenicity of available murine antibodies may hamper repeated administration of radioimmunoconjugates. Second, the pharmacokinetic properties of whole IgGs are suboptimal due to their poor diffusion into large tumour masses. Furthermore, a large variety of cancer types lack a true tumour-specific target since most tumour-associated antigens are also expressed on normal tissues, albeit at a variable cellular density.

The F16 antibody is a fully humanized antibody isolated using phage display technology [10]. It recognizes the alternatively spliced A1 domain of tenascin-C, one of the best characterized markers of angiogenesis [11]. Tenascin-C is an extracellular matrix (ECM) component that is widely expressed in a variety of normal tissues and body fluids. Different tenascin-C isoforms can be generated by alternative splicing of the tenascin-C pre-mRNA, a process that is modulated by cytokines and extracellular pH. The domains A1 to D may be included or omitted in the final tenascin-C molecule. The tenascin-C isoform containing the A1 domain is undetectable immunohistochemically in normal adult tissues, with the exception of tissues undergoing physiological remodelling (e.g. endometrium and ovary) and during wound healing. By contrast, its expression in tumours and fetal tissues is high [11, 12]. The formation of new blood vessels is a rare event in the adult (except in the female reproductive cycle), but is a pathological feature of most aggressive types of cancer. F16 localizes preferentially around tumour blood vessels while sparing normal tissues. More recently, the F16 antibody has been synthesized in the small immunoprotein (SIP) or “miniantibody” format. This recombinant antibody format (of about 80 kDa) has been shown to display superior pharmacokinetic properties in vivo compared to the smaller scFv format (of about 25 kDa) and to the IgG format (of about 150 kDa) [13].

Radiolabelled F16SIP has been extensively characterized in animal models [11] with the aim of developing it for clinical use. Early on in the development of this compound the decision was taken to use iodine isotopes as the radiolabel. This was based on data obtained with a similar compound (L19SIP) recognizing the extra-domain B of fibronectin, another component of the modified ECM [14]. The use of iodine labelling has been shown to be adequate for this application. Preclinical RIT studies have indicated that radiolabelling of L19SIP with ^{131}I yields better tumour targeting and treatment efficacy than radiolabelling with ^{177}Lu [15]. A biodistribution study comparing ^{125}I- and ^{111}In-labelled L19SIP in animals and subsequent dosimetric estimates for the ^{131}I- and ^{90}Y-labelled counterparts have shown that the best trade-off for absorbed dose between tumour, kidney and red marrow is obtained with ^{131}I-L19SIP [13]. In initial clinical evaluation of ^{131}I-L19SIP, scintigraphic studies have shown the ability of this compound to specifically concentrate in lymphoma lesions, and administration of therapeutic doses of this compound have produced objective responses in some patients [16, 17]. Recently, PET imaging with ^{124}I-labelled F16SIP has been utilized in patients with head and neck cancer and biodistribution properties have been shown to be similar to those of L19SIP [18]. All this information supports the use of ^{131}I-labelled SIPs for this radionuclide therapy trial.

The rationale for using MoAbs in HL, regardless of the expression of a given target antigen on Hodgkin and Reed-Sternberg (H-RS) cells, is that neoplastic growth is highly regulated by interactions between tumour cells and reactive cells accumulating in HL-involved tissues. These nonmalignant cells, including T cells, B cells, macrophages, eosinophils, mast cells and fibroblasts, are recruited by H-RS cells and are activated to produce soluble or membrane-bound molecules promoting tumour cell growth and survival [19, 20]. Therefore, by targeting and killing reactive cells, H-RS cells are deprived of survival/growth signals and may become more susceptible to spontaneous and/or drug-induced apoptosis. An example of the successful use of this approach is the utilization of rituximab in refractory/recurrent classical HL [21–24]. In addition to inflammatory cells, HL tissues are characterized by altered expression of a number of ECM components and by preponderant neoangiogenic processes [19, 20]. In this regard, the F16 antibody could result in efficient targeting of both cellular, i.e. fibroblasts, and

extracellular stromal components of the HL microenvironment that highly express tenascin-C. In contrast to NHLs, strong expression of tenascin-C has been documented in HL stroma, suggesting that tumour cells are able to synthesize growth factors that stimulate fibroblasts to overproduce tenascin-C [22]. Accordingly, H-RS cells have been found to express type 3 fibroblast growth factor (FGF) receptors and FGF [25]. Additional FGF receptor subtypes and vascular endothelial growth factor can be upregulated on tumour cells through paracrine stimulation from reactive cells [19, 20, 25]. Finally, H-RS cells themselves have been shown to express tenascin-C, further supporting a role of this molecule in tumour growth promotion in HL [26]. Therefore, F16-based RIT may enable the simultaneous targeting of H-RS cells, of cellular and extracellular components of the tumour microenvironment and of cellular pathways underlying the proangiogenic processes occurring in HL.

A phase I/II dose-finding and efficacy study of the tumour-targeting properties of ^{131}I-F16SIP (Tenarad) in patients with different types of malignancies has recently been completed. We report here the results of ^{131}I-F16SIP treatment in eight in patients with refractory HL accrued at our institution. Preliminary results of this study were presented at the American Society of Clinical Oncology (ASCO) annual meeting in 2011 [27].

Materials and methods

Study design and patient population

The trial discussed here was a phase I/II dose-finding and efficacy study of the human F16SIP MoAb fragment labelled with ^{131}I (Tenarad) in patients with cancer. The study, approved by the independent ethics committee of our institution as well as the regulatory national agency (EudraCT number 2007-007259-15), was a multicentre, open-label, two-step single-arm dose-escalation study in sequential cohorts of patients with cancer.

The clinical trial was designed for assessing efficacy in patients with any cancer showing progressive disease (PD) and in whom all conventional treatments had failed. We report the results obtained in eight patients enrolled at our institution with a diagnosis of HL. The main characteristics on presentation are shown in Table 1. All patients had undergone several lines of treatment prior to enrolment and presented with active PD. Once enrolled, patients underwent baseline assessment consisting of a complete blood work-up, a contrast-enhanced whole-body CT scan and a whole-body FDG PET/CT scan.

Radiolabelling

Carrier-added ^{131}I was purchased from GE Healthcare at activity concentrations ranging from 74–925 MBq/ml depending on the intended use of the final product (diagnostic study or RIT). F16SIP was labelled using the chloramine-T method. Chloramine-T was purchased from Sigma (Sigma Chemical Company, St. Louis, MI). F16SIP was obtained from Philogen SpA in 4.6 ml 50 mM sodium phosphate buffer pH 7.4. The radiolabelling procedure consisted of a controlled oxidation without the use of a reducing agent to stop the reaction. The amount of starting radioactivity utilized was calculated considering the weight of the patient and the expected labelling yield. In preliminary experiments, reaction parameters were optimized in terms of the amount of chloramine-T, precursor, temperature and time. The reaction was initiated by adding the chloramine-T solution (0.24 M, prepared immediately before labelling) directly to the reaction mixture at room temperature. The optimal time of incubation was found to be approximately 165 s. Unbound ^{131}I was removed by gel filtration using prepacked HiPrep26/10 desalting columns (GE Healthcare Eu, Freiburg, Germany) and eluted with phosphate-buffered saline (Sigma Chemical Company, St. Louis, MI). The radiolabelled antibody was sterile-filtered (0.22 μm). All the Tenarad labelling steps for both diagnostic and therapeutic applications were carried out with a semiautomated labelling module (Easy Iodine, Philogen, SpA, Italy) that allows high and reproducible yields and reduces radiation exposure for workers.

Silica gel thin-layer chromatography (mobile phase methanol/water 85:15) was utilized to assess radiochemical purity. Radiochemical yields for diagnostic and RIT preparations of ^{131}I-F16SIP were 87.50±4.63 % and 89.38±2.92 % (mean±SD), respectively. The purified reaction mixture was also evaluated for immunoreactivity by measuring radioactivity retained on an antigen affinity chromatography column. The mild reaction conditions did not appear to significantly affect antigen recognition (immunoreactivity 87.44±1.33 %).

Gamma camera imaging and dosimetry to organs at risk

A diagnostic study was performed in enrolled patients to determine eligibility for administration of the therapeutic dose. Patients were injected intravenously with 185 MBq Tenarad (4 mg). After administration, blood samples were taken and whole-body images obtained at different time-points between 30 min and up to 1 week after injection. Serial whole-body scans were acquired on an E.cam dual head gamma camera system (Siemens, Erlangen, Germany) using whole-body imaging mode, a fixed radial distance from the patient, a scan speed of 10 cm/min and the factory preset energy windows for ^{131}I. For scatter correction with the triple energy window method [28], additional narrow scatter windows were simultaneously acquired (lower adjacent window 8 % wide and upper 7 % wide). Tomographic acquisitions (64 views, 30 s per view) were acquired to assess the three-dimensional distribution of activity in selected anatomical districts. In order to be eligible to

Table 1 Patient characteristics and treatments performed prior to enrolment

Patient	Gender	Age (years)	Histotype	Stage	Year of diagnosis	Previous chemotherapy regimens	Other treatments
1/F025	F	25	Mixed cellularity	IVB	2004	ABVD, BEACOPP, CEP, LABO, IGEV, DHAP	RT; ASCT
2/F029	M	30	Nodular sclerosis	IIB	2008	BEACOPP, ESHAP, ICE, LABO, IGEV	RT; ABMT
3/F032	M	41	Nodular sclerosis	IVB	1998	ABVD, MICMA, GIFOX, bendamustine-rituximab, ESHAP	RT; RIT; ASCT; (Zevalin®)
4/F040	F	22	Nodular sclerosis	IIB	2007	ABVD, CHOP, IGEV, vinblastine	RT; ASCT
5/F044	M	28	Nodular sclerosis	IVB	2009	BEACOPP, DHAP, GEM-VIN+DEXA	RT; ASCT
6/F945	F	31	Nodular sclerosis	IVB	2006	BEACOPP, IGEV, CVPP, PEP-C, GEM-VIN	RT; ABMT
7/F046	F	21	Nodular sclerosis	IIB	2009	BEACOPP, doxorubicin, DHAP	ASCT
8/F051	M	19	Nodular sclerosis	IVB	2007	BEACOPP, IGEV, DHAP, PEP-C	RT

RT external beam radiotherapy; *ASCT* autologous peripheral stem cell transplantation; *ABMT* autologous bone marrow transplantation; *ABVD* Adriamycin, bleomycin, vinblastine, dacarbazine; *BEACOPP* bleomycin, etoposide, Adriamycin, cyclophosphamide, vincristine, procarbazine, prednisone; *CEP* CCNU (lomustine), etoposide, prednimustine; *CHOP* cyclophosphamide, hydroxydaunorubicin, vincristine, prednisone; *CVPP* cyclophosphamide, vincristine, procarbazine, prednisone; *DEXA* dexamethasone; *DHAP* dexamethasone, cytarabine, cisplatin; *ESHAP* etoposide, methylprednisolone, cytarabine, cisplatin; *GEM-VIN* gemcitabine, vincristine; *GIFOX* gemcitabine, ifosfamide, oxaliplatin; *ICE* ifosfamide, carboplatin, etoposide; *IGEV* ifosfamide, gemcitabine, vinorelbine, prednisolone; *LABO* lomustine, Adriamycin, bleomycin, vincristine; *MICMA* mitoxantrone, carboplatin, Aracytin, methylprednisolone; *PEP-C* prednisone, etoposide, procarbazine, cyclophosphamide

receive the therapeutic dose of the radioimmunoconjugate, uptake of the compound in known areas of disease had to be at least four times higher than in surrounding muscle in images acquired 24 h after injection.

Before Tenarad administration, patients underwent a transmission scan using a ^{57}Co flood source for attenuation correction. To calibrate the camera, a transmission curve with a spherical source of ^{131}I had been measured by varying the water thickness, with the same irradiation geometry as the patient acquisition scan (see the Pseudoextrapolation Number method of MIRD Pamphlet No.16 [28]).

Dosimetry to organs at risk To determine the activity in normal organs (liver, lungs, spleen, kidneys, heart wall) the conjugated-view planar imaging technique was used. Regions of interest (ROIs) were drawn on the organs and background regions. The background ROIs were usually drawn contiguous to the target ROI, and the method of Buijs et al. [29] was used for background correction. The ROI counts in the whole-body images were normalized with respect to the total counts of the first image obtained before any excretion of activity. The open source software OSIRIX (http://www.osirix-viewer.com) was used for ROI definition and analysis.

The fraction of injected activity curve for each source organ in each patient was fitted using least-squares linear regression to a monoexponential function. The area under the time–activity curve for each given organ represents the residence time. Residence times were calculated for the whole body, each source organ and the remaining body tissues. The residence time of the remaining tissues was determined by subtracting the sum of the source organ residence times from that of the whole body. The absorbed doses to the target organs were obtained considering the individual organ masses and body weight. OLINDA/EXM software [30] was used to calculate the absorbed doses (in milligrays per megabecquerel).

Dosimetry to red marrow The mean absorbed dose was calculated as the sum of the self-absorbed dose to the red marrow and the absorbed dose to the red marrow from activity in the remainder of the body. The blood-based method of Sgouros was adopted for the self dose contribution [31]. The activity in the red marrow (A_{RM}) is proportional to the radioactivity in the blood according to their mass ratio modulated through the red marrow-to-blood concentration ratio (RMBLR): $A_{RM} = RMBLR \times A_{BL} \times m_{RM}$, *where* $RMBLR = 0.19/(1 - haematocrit)$, A_{BL} is the activity in whole blood and m_{RM} is the standard red marrow mass (1,120 g in men and 1,300 g in women). The activity in samples of whole blood was measured using a Wizard 1480 gamma counter (Wallac, Turku, Finland) calibrated with known activities of ^{131}I with the same geometric conditions (volume, shape and position) used for blood sample counting. The residence time in blood was obtained by biexponential fitting of the experimental data. To obtain a more accurate value of red-marrow absorbed dose, nonlinear scaling S factors for patient-specific organ masses were applied, not only to the self-irradiation term but also to the cross-irradiation term [32]. Estimates of lesion absorbed doses were obtained in 12 lesions. The "sphere model" implemented in OLINDA-EXM was used to obtain S values for self-irradiation associated with lesions of different sizes. A uniform intralesional distribution of radioactivity was assumed to estimate the mean absorbed dose.

Treatment protocol

All patients in this cohort received 2.05 GBq/m^2 (5 – 10 mg) of ^{131}I-Tenarad for therapy. The activity was administered by slow intravenous infusion (in 100 – 200 mL saline over 30 min) while hospitalized. Patients remained hospitalized for 4 – 5 days following administration and were discharged only after levels of radiation were within legal limits imposed by national regulatory authorities. Radioiodine uptake by the thyroid was blocked by administering Lugol's solution (20 %, three to five drops three times per day) starting 3 days before administration of ^{131}I-Tenarad and up to 10 days after administration of each study drug. Additionally, potassium perchlorate capsules (200 mg) were given three times daily for the same amount of time. Thyroid function tests were performed at all subsequent follow-up visits.

All patients received one administration of the therapeutic dose of Tenarad and were monitored for response and toxicity. Two patients received one additional administration and three patients received two additional administrations of the drug, with a time interval of at least 3 months between administrations. This was in accordance with the study protocol that allowed repeat administrations in all those patients who were deemed to have obtained some clinical benefit from the treatment, based on the results of follow-up visits.

Toxicity evaluation and response assessment

Haematological and nonhaematological toxicities were monitored for 6 – 8 weeks following treatment. Guidelines for evaluating expected and unexpected toxic effects of treatment were dictated by the approved study protocol and graded according to the NCI-CTCAE v3.0 criteria (http://ctep.cancer.gov/protocolDevelopment/electronicapplications/docs/ctcaev3.pdf). Approximately 1 month and 2 months after therapy, patients also underwent a whole-body FDG PET/CT scan, a contrast-enhanced CT scan and thyroid function tests to assess response and for evaluation of thyroid dysfunction. CT scans were used to measure the diameter of lesions and FDG PET/CT was performed to assess metabolic response. Objective responses were assessed according to the 2007 Revised Criteria as reported by Cheson et al., and categorized as complete response (CR), partial response (PR), disease stabilization (SD) and relapse/PD [33].

Results

All patients were eligible to receive the therapeutic dose of ^{131}I-Tenarad, based on evidence that one or more documented disease-involved sites showed uptake on the diagnostic study at least four times greater than muscle at the 24 h time-point. The prescribed administered activities ranged from 2.85 to 4.26 GBq (2.05 GBq/m^2) for the first administration. Overall treatment results in all patients are summarized in Table 2. There was one CR (patient 2), one PR (patient 1) and five SD (patients 3, 4, 5, 6 and 8), based on the assessment after the first Tenarad administration. The remaining patient (patient 7) had rapid PD and died shortly after the first assessment when she was found to have developed new lesions.

Figure 1 shows imaging studies in patient 2. This patient had recurring disease in the neck and mediastinum and presented with highly FDG-avid disease. Images obtained 4 days after administration of the therapeutic dose of Tenarad demonstrated intense uptake of the radioconjugate in involved lymph nodes. The follow-up FDG PET scan at 1 month showed a dramatic therapeutic effect, which was consistent with CR. At 2 months after therapy, however, FDG uptake in previously involved areas was again observed, although at a significantly lower intensity than at baseline.

Of the five patients scored as SD, at least three (patients 3, 4 and 8) showed clear signs of clinical benefit from therapy: patient 3 showed a reduction in size of lung lesions and a marked reduction in FDG uptake of many bone lesions; patient 4, who presented with bulky abdominal disease and bilateral involvement of axillary lymph nodes, showed a significant reduction in FDG uptake, although a reduction in the size of nodal lesions was not sufficient to qualify for a PR; and patient 8, whose key imaging findings are summarized in Fig. 2, had cervical nodal involvement and bilateral axillary disease. These areas were highly avid for FDG on PET/CT scans. The diagnostic immunoscintigraphic study showed significant uptake of Tenarad in the largest axillary lesions and at the sternal notch. After administration of the therapeutic dose, whole-body images showed high concentrations of Tenarad in disease-involved sites. Response assessment at 1 month showed a marked reduction in intensity of FDG uptake in the axillary lymph nodes. There was also clinical evidence of improvement based on resolution of an extended nonblanching rash involving axillary areas and full functional recovery of the ability to flex, rotate and adduct shoulder and upper limbs, movements that were severely impaired before Tenarad treatment. However, given the insufficient reduction in lymph node size and persistent metabolic FDG activity, response was classified as SD. In the remaining two patients (patients 5 and 6), the treatment did not appear to significantly alter the disease course. Patient 5 had extensive bone involvement, and although a minor reduction in lymph node lesion size was observed at the first assessment, this rapidly reversed and imaging studies at the second assessment showed PD in both lymph nodes and bone. In patient 6, who had extensive lung involvement, no significant size changes in the extranodal tumour mass occurred and constitutional B

Table 2 Administered activities and response assessment

Patient	RIT number	Administered activity (GBq)	Best response[a]	Duration of response (months)	Note
1/F025	1	3.03	PR	3	Progression 5 months after RIT
	2	3.07	SD	3	Progression 4 months after RIT
	3	2.88	SD	3	Referred for different therapy
2/F029	1	4.18	CR	1	Progression 7 months after RIT
	2	3.40	SD	2	Progression 5 months after RIT
3/F032	1	3.29	SD	2	Marked reduction in areas of bone FDG uptake
	2	3.0	PD	–	Referred for different therapy
4/F040	1	2.85	SD	2	Progression 4 months after RIT
	2	2.85	SD	2	Progression 3 months after RIT
	3	2.02	SD	5	Referred for different therapy
5/F044	1	4.26	SD	1	Progression 2 months after RIT
6/F945	1	3.05	SD	3	Worsening of HL symptoms, referred for different therapy
7/F046	1	3.51	PD	–	Rapid PD, death 2 months after RIT
8/F051	1	3.33	SD	2	Progression 3 months after RIT
	2	2.66	PR	2	Progression 3 months after RIT
	3	3.03	PR	2	Referred for different therapy

[a] According to the criteria of Cheson et al. [33]

symptoms and fatigue persisted unmodified; so the treatment was considered a failure.

Repeated Tenarad treatments

Five of the eight patients (patients 1, 2, 3, 4 and 8) were considered to have received clinical benefit from administration of Tenarad. All these patients received a second therapeutic dose between 3 and 12 months following initial treatment. Prior to the second treatment all but one patient (patient 3) had evidence of new PD based on imaging and clinical findings. Patients 1, 4 and 8 also received a third therapeutic dose. For the second and third RITs the same activities (2.05 GBq/m^2) were delivered, except in patients 2 and 8, who received a 25 % reduced dose because of the haematological toxicity observed following the first therapeutic Tenarad dose. The second administration was not effective in patient 3 since early PET/CT reassessment showed increased numbers of active bone and pulmonary lesions classified as PD. All four remaining patients achieved a reduction in size and FDG standardized uptake values in at least some of the lesions after the second therapeutic dose (three SD and one PR).

Regarding the three patients receiving a third Tenarad RIT, patient eight showed PR at the first assessment, but this effect was again short-lived and recurrence in size and FDG avidity of involved nodes was evident at the second assessment (2 months after RIT) as for the previous two RITs. Patients 1 and 4 showed SD.

Toxicity

Given the high bone marrow radiation absorbed doses with this type of RIT, haematological toxicity was the main concern in the immediate post-therapy follow-up. Patients were carefully monitored with weekly full haemograms. Toxicity data following the first Tenarad administration are summarized in Table 3. As expected, moderate (G1/G2) to severe (G3) thrombocytopenia was experienced by all patients, along with G2/G3 neutropenia and lymphopenia. Maximal toxicities were observed between weeks 4 and 5 following treatment and generally resolved without the need for specific intervention. In contrast, a single patient (patient 2) showed severe (G4) multilineage haematological toxicity with nadirs for platelets and neutrophils (11,000/μL and 300/μL, respectively) occurring 5 weeks after administration of the first Tenarad dose (4.18 GBq), despite not having bone marrow involvement. This patient was hospitalized and required platelet transfusion and growth factors. It should be noted that these patients were heavily pretreated and in several instances, although complying with inclusion criteria, haematological values were below the lower limits of normal at initial work-up.

Although every effort was made to reduce radioiodine uptake in the thyroid by giving cold iodide and perchlorate, four patients developed hypothyroidism during follow-up and

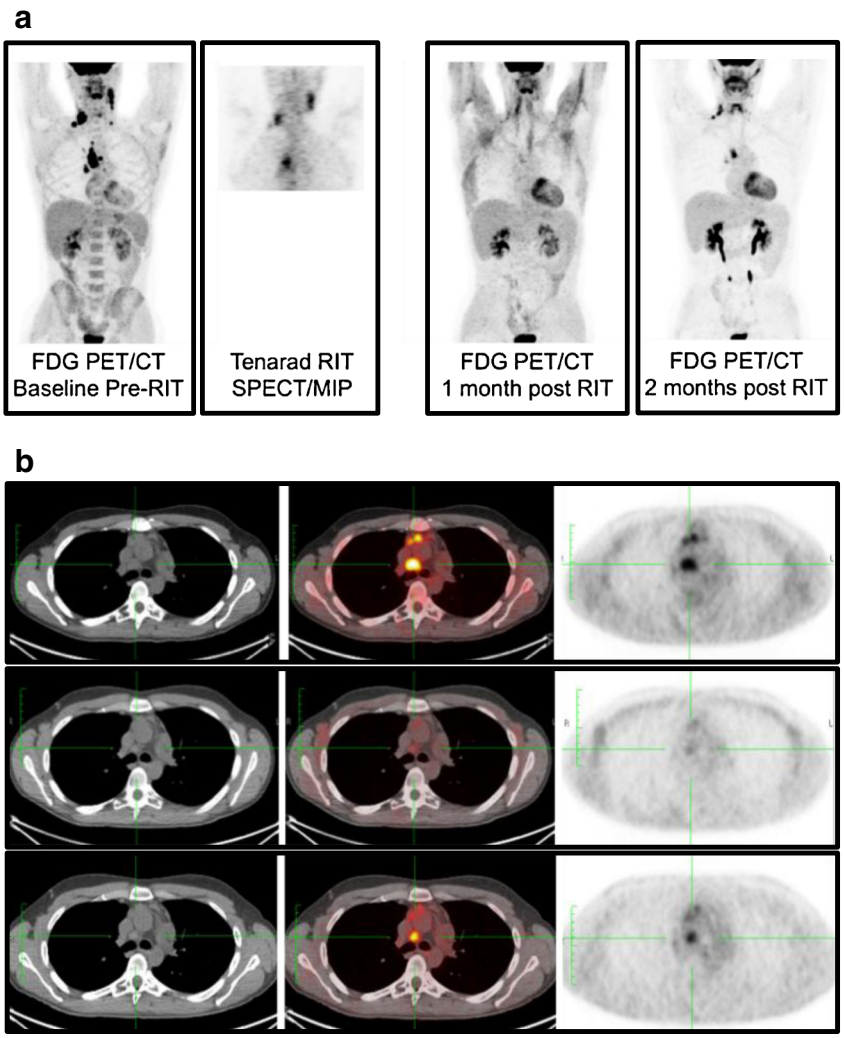

Fig. 1 Imaging in patient 2. **a** *left* Maximum intensity projection (MIP) image of the baseline FDG PET scan shows active disease in the neck and mediastinum; *centre left* SPECT MIP image acquired 4 days after administration of the therapeutic dose shows high concentrations of Tenarad in known areas of disease; *centre right* and *right* response assessment FDG PET/CT images acquired 1 month (*centre right*) and 2 months (*right*) after treatment show marked reductions in FDG uptake in known areas of disease. **b** *top row* Transaxial FDG PET/CT images of precarinal nodes at baseline; *middle row* and *bottom row* FDG PET/CT images acquired after treatment show CR at the first assessment (*middle row*) and partial metabolic recovery at the second assessment (*bottom row*)

were placed on thyroid hormone supplementation. All four patients who developed hypothyroidism had received at least two therapeutic doses of Tenarad.

Organs at risk and lesion dosimetry

Biodistribution analysis of Tenarad was performed in all eight patients by analysing the pretherapy imaging and blood sample data. Mean estimated doses to organs at risk and to lesions are shown in Table 4. Average absorbed doses per unit activity are shown in Fig. 3. The red marrow showed an average absorbed dose of approximately 0.3 Gy that is well below what is considered dose limiting (2 Gy) in RIT studies. Thyroid absorbed doses were higher and highly variable and were based on posttherapy imaging as this was deemed to be more accurate (Table 4). The thyroid blockade regimen used was not completely effective or compliance was poor in some patients. Estimates of absorbed doses were obtained in 12 lesions. Although there was evidence of some treatment efficacy, the overall lesion absorbed dose estimates were fairly low with a maximum of 16.5 Gy.

Discussion

The relevance of the tumour microenvironment to the evolution and progression of different types of human cancers has provided the basis for envisaging alternative treatment strategies aimed at the therapeutic targeting of cellular and extracellular components of the neoplastic stroma. ECM proteins and newly formed blood vessels may be ideal targets for cancer RIT for different reasons [34]. There are certain ECM proteins, in particular specific domains generated by alternative mRNA splicing, that are specific to the neovasculature of tumours. The tenascin-C isoform containing the A1 domain, specifically targeted by the radioimmunoconjugate used in this study, is one such molecule. This particular isoform, undetectable in most normal adult tissues, is markedly overexpressed in many tumours, thus making it a worthwhile

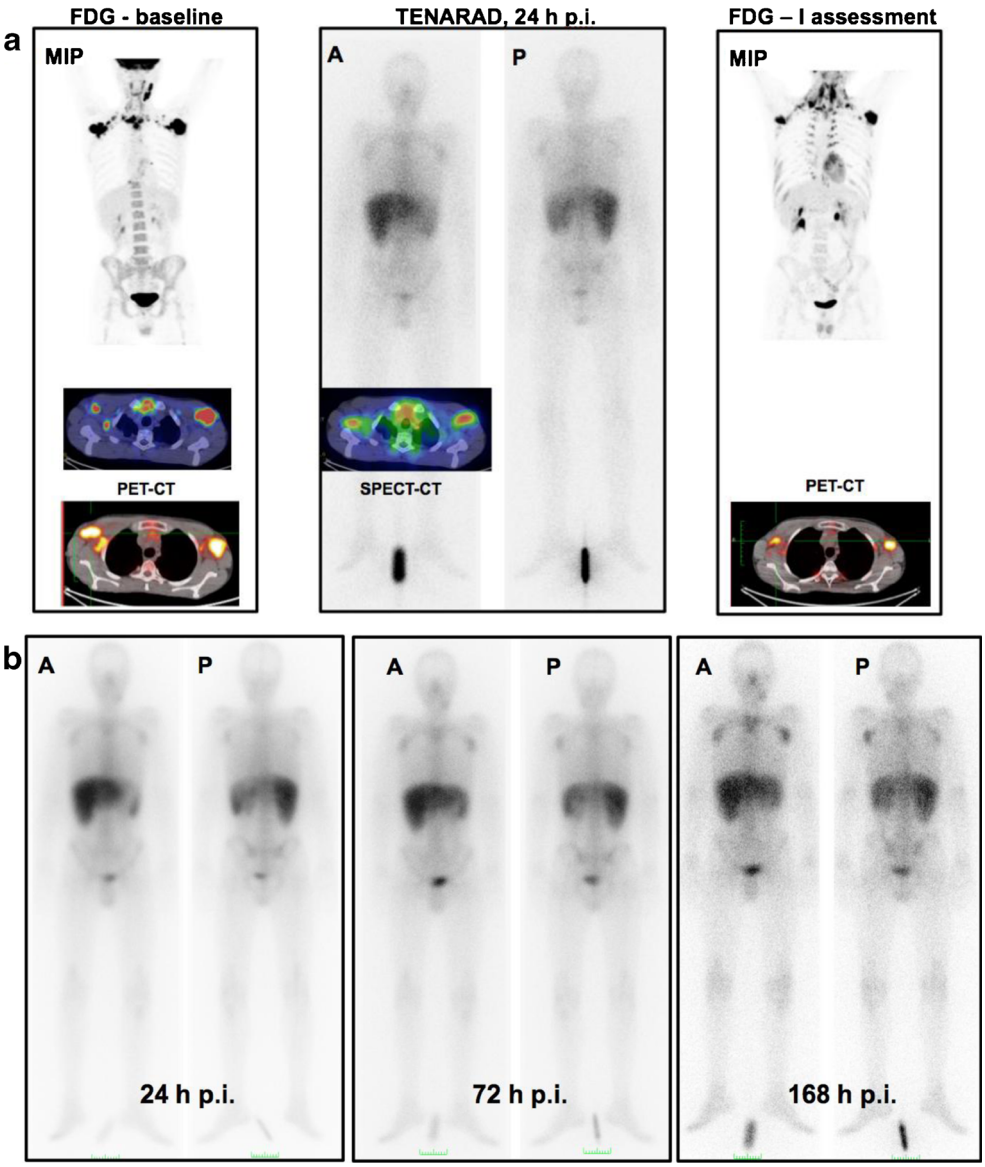

Fig. 2 Imaging in patient 8. **a** *left* Maximum intensity projection image of the baseline FDG PET/CT scan shows intense uptake in the axillae and at the sternal notch as well as in some cervical nodes; *centre* diagnostic image acquired 24 h after injection of the radioimmunoconjugate shows uptake of Tenarad in the axillary nodes (comparison of the fused PET/CT and SPECT/CT images confirms colocalization of Tenarad and the areas of increased FDG uptake); *right* PET/CT image acquired 4 weeks after the first treatment shows a reduction in FDG uptake. **b** Whole-body planar images (*A* anterior view, *P* posterior view) acquired at different times after administration of the therapeutic dose (3.33 GBq) with increasing contrast in Tenarad accumulation in the known areas of disease compared to other organs. This patient was scored as SD based on the criteria of Cheson et al.

Table 3 Disease characteristics and haematological toxicities

Patient	Disease-involved sites	Toxicity grade[a]			
		Thrombocytopenia	Leucocytopenia	Neutropenia	Lymphopenia
1/F025	Lymph nodes/extranodal disease (liver and bone)	3	1	1	2
2/F029	Lymph nodes	4	4	4	4
3/F032	Lymph nodes/extranodal disease (lung, liver, spleen, bone)	2	2	2	2
4/F040	Lymph nodes	3	3	3	3
5/F044	Lymph nodes/extranodal disease (bone)	1	NA	NA	2
6/F945	Lymph nodes/extranodal disease (lung)	3	1	NA	NA
7/F046	Lymph nodes/extranodal disease (lung, bone)	2	3	NA	NA
8/F051	Lymph nodes	2	1	1	1

NA not available

[a] The highest grade of toxicity for each parameter which was reached at week 4 or 5 is shown

Table 4 Absorbed doses to organs at risk and lesions (mean and corresponding ranges) derived from Tenarad pretreatment dosimetry

	Absorbed dose (Gy)	
	Mean±SD	Range
Organs at risk		
Kidneys	2.42±0.51	1.94 – 3.46
Spleen	2.09±1.02	0.94 – 3.27
Liver	1.88±0.81	0.92 – 3.13
Lungs	0.91±0.29	0.53 – 1.36
Heart wall	0.73±0.12	0.57 – 0.90
Total body	0.38±0.09	0.27 – 0.48
Red marrow	0.31±0.05	0.22 – 0.36
Thyroid[a]	6.1±5.2	0.28 – 12.1
Lesions (n=12)	6.0±4.9	1.70 – 16.5

[a] Thyroid absorbed dose estimates were based on posttherapy imaging studies

target to pursue for cancer therapy [11, 12]. The fact that tenascin-C is abundantly concentrated in the areas surrounding cancer cells and in proximity to fenestrated capillaries and vessels present in the tumour, facilitates diffusion and targeting of compounds, such as the intermediate molecular weight protein (F16SIP) used in this study, to their specific binding sites. Thus, intrinsic features of the selected target contribute to achieving high target binding and improved radionuclide concentrations in areas where the antigen is expressed.

The rationale for testing the clinical activity of Tenarad in HL is further supported by some specific features of this tumour. HL is a prototype malignancy in which survival and proliferation of the neoplastic H-RS cells are strictly dependent on stimulatory signals provided by surrounding inflammatory cells and by ECM proteins abnormally distributed within the tumour stroma [19, 20]. Such abnormal deposition of ECM mimics in part the normal wound-healing process and is associated with a preponderant neoangiogenic process [19, 20, 22, 25, 26, 35, 36]. Specifically, the HL microenvironment is characterized by the abundant presence of fibroblasts that are stimulated by cytokines derived from H-RS cells, such as FGF and connective tissue growth factor, to overproduce tenascin-C [25, 35, 36]. Accordingly, expression of tenascin-C in HL tissues is significantly higher than in NHL tissues [22]. In addition, the presence of a vigorous proangiogenic milieu providing high levels of neovessel-associated tenascin-C is a typical feature of the HL microenvironment [19, 20, 25]. Finally, tumour cells themselves constitutively express and secrete tenascin-C [26]. So, clinical administration of Tenarad in HL may result in the simultaneous targeting of malignant H-RS cells and of multiple components of the tumour-supporting microenvironment including fibroblasts and neovessels.

Our early clinical results support the therapeutic potential of Tenarad in patients with refractory HL and should prompt further studies in this malignancy. A single administration of Tenarad achieved objective responses in most patients including one CR, one PR and five SD, with only one patient showing PD shortly after treatment. This response rate, although not apparently impressive, adequately compares with other experimental single-agent treatments used in this highly unfavourable population of patients [37, 38]. In this regard, all patients were extensively pretreated with chemotherapy and external beam RT, and 75 % of them had also received a prior ASCT. Interestingly, however, haematological toxicity was acceptable, never life-threatening and spontaneously resolved in most patients without the need for growth factor support or blood cell transfusions (which were necessary only in one patient). We did observe a decline in thyroid function in several patients despite blocking radioiodine uptake through administration of cold iodide and perchlorate. It is unclear whether this was due to inadequacy of the thyroid blockade scheme or, more likely, to poor compliance with taking the thyroid-blocking drugs. We observed radioiodine uptake in the thyroid in all patients in the whole-body images acquired several days after administration of the therapeutic dose of Tenarad. Notably, however, all patients who developed hypothyroidism had received two treatments leading to a fairly high cumulative dose of Tenarad (5.3 – 7.6 GBq).

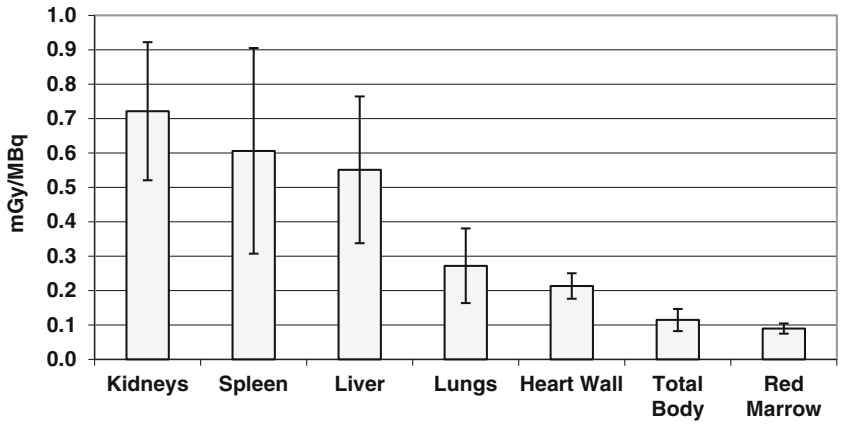

Fig. 3 Mean absorbed doses per unit of injected activity to organs at risk (*error bars* SD) derived from Tenarad pretreatment dosimetry

The responses obtained were short-lived in most patients, suggesting that more effective ways of administering Tenarad should be explored. One possible approach may be fractionation of the radioactivity delivered, as opposed to the single administration design of this study, as shown in other schemes of radionuclide therapy [39]. Another potential approach may be combination treatment with newer target-based biological agents known to be effective in HL. These latter molecules need time to fully exert their biological actions and, given their moderate single-agent activity, need to be combined with other agents to maximize their therapeutic potential [6, 37, 38]. Since several of these agents, such as lenalidomide, tyrosine kinase inhibitors, histone deacetylase inhibitors and some MoAbs, are known to specifically target proangiogenic pathways, their combination with Tenarad may be of value in HL [6, 37, 38].

Conclusion

The present study provides a proof-of-concept translational approach to test the hypothesis that targeting tenascin-C expressed in the HL microenvironment may be a useful way to specifically deliver appropriate radiation doses to disease-involved tissue sites. In heavily pretreated HL patients with a poor prognosis, Tenarad RIT showed acceptable toxicity and in some patients produced objective responses and adequate disease control in a population with limited therapeutic options available. Multiple administrations of Tenarad and, probably, schedule modifications, may be necessary to improve treatment efficacy and response duration with this form of RIT.

Acknowledgments Philogen SpA sponsored this work under a protocol approved by the internal review board of our institution.

Conflicts of interest None of the authors from the Istituto Nazionale Tumori, Fondazione "G. Pascale", Napoli, Italy, received compensation for this study and none declare conflicts of interest. The remaining authors (D.N., L.G. and H.D.M.) are shareholders or employees of the protocol sponsor, Philogen SpA.

References

1. Bauer K, Skoetz N, Monsef I, Engert A, Brillant C. Comparison of chemotherapy including escalated BEACOPP versus chemotherapy including ABVD for patients with early unfavourable or advanced stage Hodgkin lymphoma. Cochrane Database Syst Rev. 2011:(8): CD007941. doi:10.1002/14651858.CD007941.pub2
2. Kuruvilla J, Keating A, Crump M. How I treat relapsed and refractory Hodgkin lymphoma. Blood. 2011;117:4208–17.
3. Uhm J, Kuruvilla J. Treatment of newly diagnosed advanced stage Hodgkin lymphoma. Blood Rev. 2012;26:167–74.
4. Brice P. Managing relapsed and refractory Hodgkin lymphoma. Br J Haematol. 2008;141:3–13.
5. Horning S, Fanale M, deVos S, Borchmann P, Illidge T, Engert A, et al. Defining a population of Hodgkin lymphoma patients for novel therapeutics: an international effort [abstract 118]. Ann Oncol. 2008;19 Suppl 4:120–1
6. Younes A. Novel treatment strategies for patients with relapsed classical Hodgkin lymphoma. Hematology Am Soc Hematol Educ Program. 2009:507–19. doi:10.1182/asheducation-2009.1.507
7. Illidge T, Morschhauser F. Radioimmunotherapy in follicular lymphoma. Best Pract Res Clin Haematol. 2011;24:279–93.
8. Kaminski MS, Tuck M, Estes J, Kolstad A, Ross CW, Zasadny K, et al. 131I-tositumomab therapy as initial treatment for follicular lymphoma. N Engl J Med. 2005;352:441–9.
9. Scholz CW, Pinto A, Linkesch W, Linden O, Viardot A, Keller U, et al. (90)Yttrium-ibritumomab-tiuxetan as first-line treatment for follicular lymphoma: 30 months of follow-up data from an international multicenter phase II clinical trial. J Clin Oncol. 2013;31:308–13.
10. Silacci M, Brack S, Schirru G, Marlind J, Ettorre A, Merlo A, et al. Design, construction, and characterization of a large synthetic human antibody phage display library. Proteomics. 2005;5:2340–50.
11. Brack SS, Silacci M, Birchler M, Neri D. Tumor-targeting properties of novel antibodies specific to the large isoform of tenascin-C. Clin Cancer Res. 2006;12:3200–8.
12. Borsi L, Carnemolla B, Nicolo G, Spina B, Tanara G, Zardi L. Expression of different tenascin isoforms in normal, hyperplastic and neoplastic human breast tissues. Int J Cancer. 1992;52:688–92.
13. Berndorff D, Borkowski S, Sieger S, Rother A, Friebe M, Viti F, et al. Radioimmunotherapy of solid tumors by targeting extra domain B fibronectin: identification of the best-suited radioimmunoconjugate. Clin Cancer Res. 2005;11:7053s–63s.
14. Pini A, Viti F, Santucci A, Carnemolla B, Zardi L, Neri P, et al. Design and use of a phage display library. Human antibodies with subnanomolar affinity against a marker of angiogenesis eluted from a two-dimensional gel. J Biol Chem. 1998;273:21769–76.
15. Tijink BM, Neri D, Leemans CR, Budde M, Dinkelborg LM, Stigter-van Walsum M, et al. Radioimmunotherapy of head and neck cancer xenografts using 131I-labeled antibody L19-SIP for selective targeting of tumor vasculature. J Nucl Med. 2006;47:1127–35.
16. Erba PA, Sollini M, Orciuolo E, Traino C, Petrini M, Paganelli G, et al. Radioimmunotherapy with radretumab in patients with relapsed hematologic malignancies. J Nucl Med. 2012;53:922–7.
17. Sauer S, Erba PA, Petrini M, Menrad A, Giovannoni L, Grana C, et al. Expression of the oncofetal ED-B-containing fibronectin isoform in hematologic tumors enables ED-B-targeted 131I-L19SIP radioimmunotherapy in Hodgkin lymphoma patients. Blood. 2009;113:2265–74.
18. Heuveling DA, de Bree R, Vugts DJ, Huisman MC, Giovannoni L, Hoekstra OS, et al. Phase 0 microdosing PET study using the human mini antibody F16SIP in head and neck cancer patients. J Nucl Med. 2013;54:397–401.
19. Aldinucci D, Gloghini A, Pinto A, De Filippi R, Carbone A. The classical Hodgkin's lymphoma microenvironment and its role in promoting tumour growth and immune escape. J Pathol. 2010;221:248–63.
20. Steidl C, Connors JM, Gascoyne RD. Molecular pathogenesis of Hodgkin's lymphoma: increasing evidence of the importance of the microenvironment. J Clin Oncol. 2011;29:1812–26.
21. Oki Y, Younes A. Does rituximab have a place in treating classic Hodgkin lymphoma? Curr Hematol Malig Rep. 2010;5:135–9.
22. Soini Y, Alavaikko M, Lehto VP, Virtanen I. Tenascin in reactive lymph nodes and in malignant lymphomas. Pathol Res Pract. 1992;188:1078–82.
23. Younes A, Oki Y, McLaughlin P, Copeland AR, Goy A, Pro B, et al. Phase 2 study of rituximab plus ABVD in patients with newly diagnosed classical Hodgkin lymphoma. Blood. 2012;119:4123–8.
24. Younes A, Romaguera J, Hagemeister F, McLaughlin P, Rodriguez MA, Fiumara P, et al. A pilot study of rituximab in patients with recurrent, classic Hodgkin disease. Cancer. 2003;98:310–4.

25. Khnykin D, Troen G, Berner JM, Delabie J. The expression of fibroblast growth factors and their receptors in Hodgkin's lymphoma. J Pathol. 2006;208:431–8.
26. Wallentine JC, Kim KK, Seiler 3rd CE, Vaughn CP, Crockett DK, Tripp SR, et al. Comprehensive identification of proteins in Hodgkin lymphoma-derived Reed-Sternberg cells by LC-MS/MS. Lab Invest. 2007;87:1113–24.
27. Aloj L, D'Ambrosio L, Aurilio M, Marreno R, Menssen HD, Giovannoni L, et al. Preliminary evaluation of radioimmunotherapy with Tenarad, a I-131 labeled antibody fragment targeting the extra-domain A1 of tenascin-C, in patients with refractory Hodgkin lymphoma. Journal of Clinical Oncology, 2011 ASCO Annual Meeting Abstracts. Vol 29, No. 15 suppl, 8063; 2011.
28. Siegel JA, Thomas SR, Stubbs JB, Stabin MG, Hays MT, Koral KF, et al. MIRD pamphlet no. 16: Techniques for quantitative radiopharmaceutical biodistribution data acquisition and analysis for use in human radiation dose estimates. J Nucl Med. 1999;40:37S–61S.
29. Buijs WC, Siegel JA, Boerman OC, Corstens FH. Absolute organ activity estimated by five different methods of background correction. J Nucl Med. 1998;39:2167–72.
30. Stabin MG, Sparks RB, Crowe E. OLINDA/EXM: the second-generation personal computer software for internal dose assessment in nuclear medicine. J Nucl Med. 2005;46:1023–7.
31. Sgouros G. Bone marrow dosimetry for radioimmunotherapy: theoretical considerations. J Nucl Med. 1993;34:689–94.
32. Traino AC, Ferrari M, Cremonesi M, Stabin MG. Influence of total-body mass on the scaling of S-factors for patient-specific, blood-based red-marrow dosimetry. Phys Med Biol. 2007;52:5231–48.
33. Cheson BD, Pfistner B, Juweid ME, Gascoyne RD, Specht L, Horning SJ, et al. Revised response criteria for malignant lymphoma. J Clin Oncol. 2007;25:579–86.
34. Folkman J. The role of angiogenesis in tumor growth. Semin Cancer Biol. 1992;3:65–71.
35. Birgersdotter A, Baumforth KR, Porwit A, Sjoberg J, Wei W, Bjorkholm M, et al. Inflammation and tissue repair markers distinguish the nodular sclerosis and mixed cellularity subtypes of classical Hodgkin's lymphoma. Br J Cancer. 2009;101:1393–401.
36. Birgersdotter A, Baumforth KR, Wei W, Murray PG, Sjoberg J, Bjorkholm M, et al. Connective tissue growth factor is expressed in malignant cells of Hodgkin lymphoma but not in other mature B-cell lymphomas. Am J Clin Pathol. 2010;133:271–80.
37. Buglio D, Georgakis G, Younes A. Novel small-molecule therapy of Hodgkin lymphoma. Expert Rev Anticancer Ther. 2007;7:735–40.
38. Jona A, Younes A. Novel treatment strategies for patients with relapsed classical Hodgkin lymphoma. Blood Rev. 2010;24:233–8.
39. Kwekkeboom DJ, de Herder WW, Kam BL, van Eijck CH, van Essen M, Kooij PP, et al. Treatment with the radiolabeled somatostatin analog [177 Lu-DOTA 0, Tyr3]octreotate: toxicity, efficacy, and survival. J Clin Oncol. 2008;26:2124–30.